

Efficient-VLN: A Training-Efficient Vision-Language Navigation Model

Duo Zheng Shijia Huang Yanyang Li Liwei Wang[‡]
 The Chinese University of Hong Kong
<https://lavi-lab.github.io/Efficient-VLN>

Abstract

Multimodal large language models (MLLMs) have shown promising potential in Vision-Language Navigation (VLN). However, their practical development is severely hindered by the substantial training overhead. We recognize two key issues that contribute to the overhead: (1) the quadratic computational burden from processing long-horizon historical observations as massive sequences of tokens, and (2) the exploration-efficiency trade-off in DAgger, i.e., a data aggregation process of collecting agent-explored trajectories. While more exploration yields effective error-recovery trajectories for handling test-time distribution shifts, it comes at the cost of longer trajectory lengths for both training and inference. To address these challenges, we propose **Efficient-VLN**, a training-efficient VLN model. Specifically, to mitigate the token processing burden, we design two efficient memory mechanisms: a progressive memory that dynamically allocates more tokens to recent observations, and a learnable recursive memory that utilizes the key-value cache of learnable tokens as the memory state. Moreover, we introduce a dynamic mixed policy to balance the exploration-efficiency trade-off. Extensive experiments show that Efficient-VLN achieves state-of-the-art performance on R2R-CE (64.2% SR) and RxR-CE (67.0% SR). Critically, our model consumes merely 282 H800 GPU hours, demonstrating a dramatic reduction in training overhead compared to state-of-the-art methods.

1. Introduction

Building autonomous robots that can perceive, understand, and intelligently interact with the physical world represents a long-standing goal in artificial intelligence. A critical aspect is the ability to navigate following human’s natural language instructions, playing a pivotal role in diverse practical scenarios, such as fulfilling domestic tasks, navigating complex warehouses, and rescuing in hazardous environments. To address this challenge, the task of Vision-Language

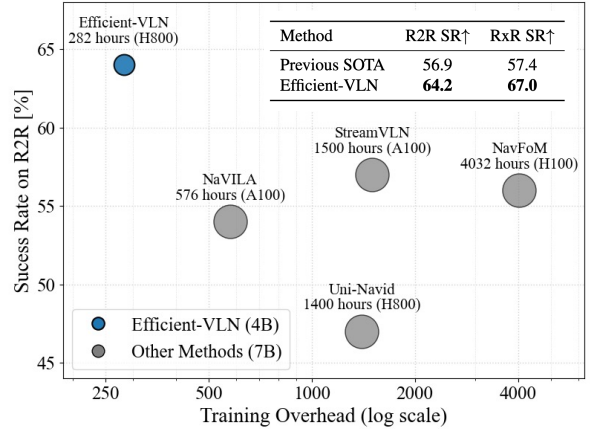


Figure 1. Efficient-VLN sets a new state-of-the-art in Vision-Language Navigation in Continuous Environments using only RGB inputs. We compare the Success Rate (SR) on the R2R-CE benchmark (y-axis) against training overhead in GPU hours (x-axis, log scale). The size of each bubble represents the relative model size. Our method achieves 64.2% R2R SR and 67.0% RxR SR, surpassing previous state-of-the-art methods. Notably, Efficient-VLN achieves this using only 282 H800 GPU hours, a fraction of the compute required by competing methods.

Navigation (VLN) [2, 19, 21, 25, 29] has emerged as a fundamental research problem, garnering extensive interest [5, 7, 10, 20, 41–43, 46, 49] from the community.

A prominent line of recent work [10, 23, 35, 41, 43, 49] tackles this problem by extending multimodal large language models (MLLMs) to this field, via modeling the historical observations as video inputs. Benefiting from the inherent world knowledge and generalizability, this paradigm has demonstrated superior performance and significant promise. Nevertheless, training these MLLM-based models presents a substantial challenge owing to their immense training overhead. As shown in Figure 1, the training of StreamVLN [35] and NavFoM [42] required 1,500 A100 and 4,032 H100 GPU hours, respectively. This substantial training overhead hinders researchers, especially those with limited computational budgets, from training advanced VLN models.

[‡] corresponding author

In this work, we focus on two key issues contributing to this challenge. First, VLN models involve processing extensive historical observations. These observations are tokenized into a sequence of tokens whose length is often excessively large, due to either accumulating all temporal steps [41] or using dense per-frame visual tokens [10, 35]. As a result, this massive token count imposes a quadratic computational burden and dominates the overall training overhead. Second, to enhance error recovery, the previous work [19, 35] employs DAGger, which collects off-policy trajectories based on a mixed policy. Specifically, the mixed policy selects the oracle or learned policy based on a fixed ratio, to generate the executed actions. A high ratio of learned policy-generated actions drives the deviation from the correct path, and this benefits learning to handle the test-time distribution shift. However, it also results in substantially longer exploration trajectories and even task failure, thus raising the training overhead.

To address the above issues, we propose a training-efficient VLN model, namely Efficient-VLN. First, to tackle the computational overhead of processing massive memory tokens, we introduce two novel efficient memory representations. (1) A progressive memory representation is constructed via a progressive spatial compression, which is inspired by the human forgetting mechanism (*i.e.*, diminishing of memories over time). Specifically, it applies a low compression ratio to visual tokens from recent frames, while gradually increasing this ratio for temporally distant ones. (2) A learnable recursive memory utilizes the KV cache of a set of learnable tokens to serve as the memory state. By propagating the memory state across consecutive steps, the memory is recursively updated while maintaining a fixed size. To enrich these representations, we integrate 3D geometry information into 2D appearance visual features. This 3D geometry information is extracted by a 3D geometry encoder (*e.g.*, StreamVGGT [53]) from raw RGB videos, without requiring explicit depth sensors or maps. Second, we introduce a dynamic mixed policy to better balance the exploration-efficiency trade-off in DAGger. Specifically, this policy starts with the learned policy for accumulating the compounding errors, and then progressively shifts towards the oracle policy to ensure eventual task completion. This design enables the collection of error-recovery data without incurring excessively long trajectories, thus accelerating the training process.

We evaluate our method on widely used VLN benchmarks, including R2R-CE [19] and RxR-CE [21]. The proposed model achieves state-of-the-art performance with a 64.2% SR on R2R-CE and 67.0% SR on RxR-CE, while consuming merely 282 H800 GPU hours, which is far less than competing methods (Figure 1). Our experiments reveal several interesting findings:

- The progressive memory representation excels at the

long-horizon RxR-CE benchmark, and demonstrates continued improvement as the memory window increases.

- The recursive memory performs well on short trajectories (R2R-CE) but struggles on longer ones (RxR-CE), demonstrating the challenge of maintaining long-term memory for state-based models.
- By utilizing the dynamic mixed policy, we achieve higher SR with a 56% reduction in exploration overhead.

2. Related Work

Vision-Language Navigation (VLN). VLN [2, 19, 21, 25, 29] represents a fundamental challenge in embodied AI, with prior work [5–7, 12, 20, 32, 46] encompassing various techniques, such as multi-task learning [43, 46, 52], specialized memory structures [7, 13, 32, 34], and data augmentation [28, 31, 38]. Our recursive memory approach is closely related to VLN \odot BERT [12], which pioneers the use of a recursive state token to compress history. It employs a single state token that is continuously processed by a BERT-style architecture. However, this poses significant challenges for gradient propagation in deep, multi-layer MLLMs. We address this limitation by introducing a novel recursive mechanism based on the KV cache. Another closely related work is CorrectNav [38], which generates error-recovery data with an LLM-based framework and iteratively bootstraps the model. However, this approach’s reliance on LLM queries incurs additional cost, whereas our approach does not require external tools.

MLLMs for Navigation. Recent research [10, 23, 34, 35, 41, 43, 46, 49] in VLN has focused on adapting Multimodal Large Language Models (MLLMs) for embodied navigation to leverage their inherent generalizability to unseen environments. Several studies [23, 49] explore employing proprietary MLLMs as navigation agents in a zero-shot setting. More recent efforts [10, 34, 35, 41, 43, 46] have shifted towards training specialized models that leverage advanced MLLMs as the backbone. NaviLLM [46] and NaVid [41] pioneer the development of trainable MLLM-based models in embodied navigation. Subsequently, NaVILA [10] introduces hierarchical agents that decouple high-level planning from low-level execution, while StreamVLM [35] enhances inference efficiency using a non-overlapping sliding window mechanism. Despite the significant progress, these methods are often constrained by substantial training overhead. The primary objective of this work is to propose a framework for training-efficient VLN models.

MLLMs for Spatial Intelligence. Understanding the 3D world from video inputs is a cornerstone of spatial intelligence and has attracted widespread academic interest [9, 37, 47, 48]. Some approaches [9, 48] enhance the perception of 3D scenes by integrating explicit 3D information

into MLLMs. Another line of work [36, 47] draws inspiration from the success of 3D geometry model [22, 30, 53], and enhances spatial reasoning by integrating latent 3D tokens extracted from RGB frames into their visual representation, obviating the necessity for 3D sensor inputs. While these studies [36, 47] primarily focus on static scene understanding, *i.e.*, from offline videos of static scenes, our work extends this paradigm to handle the real-time dynamic observations in the navigation process. A concurrent work, JanusVLN [39], also explores adapting this paradigm to VLN. Our approach further distinguishes itself by focusing on efficient memory representations and data collection strategies for error correction.

3. Method

3.1. Overview

Task Formalization. In the Vision-Language Navigation (VLN) task, a model is tasked with navigating to a target location following a language instruction I . At each step t , the model receives a new image v_t as the current observation and predicts the next sequence of actions conditioned on the instruction I and the full observation history $\{v_1, v_2, \dots, v_t\}$. Following the previous work [35, 43], the model is asked to predict the next four actions from a discrete action space comprising *forward*, *left*, *right*, and *stop*. An episode terminates when the model produces the *stop* action.

Architecture. Our model consists of three components: a visual encoder, a 3D geometry encoder, and an MLLM backbone. The workflow at step t involves the following three steps. First, the current observation v_t is encoded into a geometry-enhanced visual representation \mathbf{f}_t , which fuses conventional 2D visual features with 3D geometry features from the 3D geometry encoder. Then, the textual embeddings of the instruction I , the current geometry-enhanced visual representation \mathbf{f}_t , and the memory representation are provided to the MLLM backbone to generate the action sequence. Last, the memory representation is updated with this new visual representation (\mathbf{f}_t) to maintain crucial information.

We first describe the geometry-enhanced visual representation in Section 3.2, and then present two novel training-efficient memory representations in Section 3.3. Finally, we detail our training strategy and propose a dynamic mixed policy to enhance the DAgger algorithm in Section 3.4.

3.2. Geometry-Enhanced Visual Representation

Understanding the geometric structure of a 3D scene is crucial for recalling previously observed landmarks and achieving accurate spatial localization. However, prior

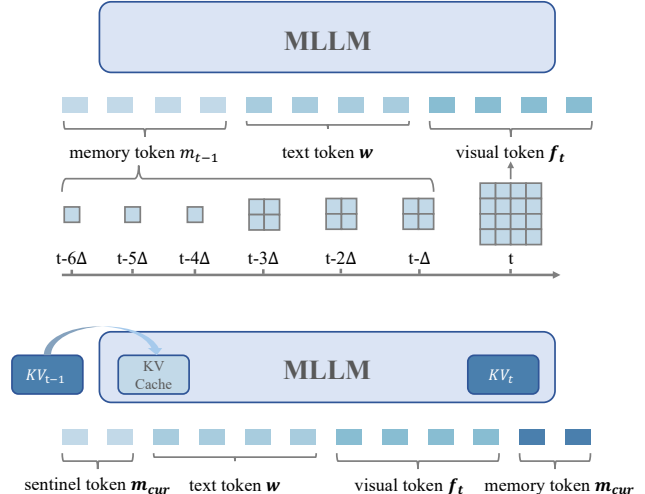


Figure 2. Illustrations of two distinct memory paradigms designed for MLLMs. (Top) The progressive memory representation allocates tokens based on temporal recency. (Bottom) The recursive memory representation maintains memory state by utilizing the KV cache of sentinel tokens to preserve crucial information.

MLLM-based approaches [10, 35, 41] have predominantly focused on processing RGB frame sequences and overlooked the explicit modeling of geometry information for 3D scenes. To address this limitation, our work enriches the visual representation by injecting 3D geometry information extracted by a 3D geometry encoder into the conventional 2D visual features. A 3D geometry encoder typically estimates geometric attributes (e.g., depth) directly from RGB images, thereby eliminating the requirement for dedicated depth sensors or pre-built maps.

2D Visual Encoding. Given an RGB image v_t at step t , the model first employs the visual encoder to convert each image $v_t \in \mathbb{R}^{h \times w \times 3}$ into a series of visual tokens $\hat{\mathbf{v}}_t \in \mathbb{R}^{\lfloor \frac{h}{p} \rfloor \times \lfloor \frac{w}{p} \rfloor \times c}$, where p represents the patch size. In this work, our model is built upon Qwen2.5-VL [4], which further compresses the visual features by grouping spatially adjacent 2×2 tokens into a single visual token. This process yields the final 2D visual representation $\mathbf{v}_t \in \mathbb{R}^{\lfloor \frac{h}{2p} \rfloor \times \lfloor \frac{w}{2p} \rfloor \times c}$.

Incorporating 3D Geometry into 2D Visual Representation. Then, we follow [47] to employ a 3D geometry model to extract the geometry information from raw RGB frame sequences. StreamVGGT is adopted in our work, as it is designed for streaming processing, and thus capable of handling dynamically updating observations. Despite this, the growing frame count causes extensive memory costs. To mitigate this problem, we evict the key-value states of a random frame (excluding the reference frame) from the cache if the number of cached frames exceeds the prede-

finer limit StreamVGGT receives the current observation v_t , and produces 3D geometry latent tokens by reusing the KV cache of past images. Subsequently, these 3D geometry latent tokens are processed through a 2-layer MLP to align them with the 2D visual representation, resulting in the final 3D geometry representation $\mathbf{g}_t \in \mathbb{R}^{\lfloor \frac{h}{2^p} \rfloor \times \lfloor \frac{w}{2^p} \rfloor \times c}$. Finally, the 2D visual representation \mathbf{v}_t and the 3D geometry representation \mathbf{g}_t are fused via element-wise addition, yielding the geometry-enhanced visual representation, denoted as $\mathbf{f}_t = \mathbf{v}_t + \mathbf{g}_t$.

3.3. Training-Efficient Memory Representation

Existing approaches [35, 41, 43] leveraging advanced MLLMs often impose a significant training overhead due to processing a massive number of visual tokens. For example, in each training step, NaVILA [10] processes 8 frames and consumes up to $196 \times 8 = 1568$ tokens, while StreamVLN [35] utilizes up to $196 \times 16 = 3136$ tokens for its visual inputs. To this end, we propose a two-fold strategy. First, we apply a general temporal sampling technique to reduce frame-level redundancy. Second, building upon this sampled history, we introduce two novel and efficient memory representations: progressive memory representation and recursive memory representation. These representations, illustrated in Figure 2, are designed to further reduce token consumption and accelerate the training process.

Temporal Sampling. Since adjacent frames often contain visually correlated content, processing these frames generates an excessive number of visual tokens and introduces significant computational redundancy. To reduce such redundancy, we apply temporal sampling by uniformly selecting frames from the sequence at a stride Δ .

Progressive Memory Representation Inspired by human forgetting mechanisms, which allocate greater resources to recent memories and progressively fewer to older ones, we introduce a progressive memory representation. This approach simulates the forgetting process by applying spatial compression to visual tokens of past observations. Given the visual features of sampled frames $\{\dots, \mathbf{f}_{t-2\Delta}, \mathbf{f}_{t-\Delta}, \mathbf{f}_t\}$, where $\mathbf{f}_i \in \mathbb{R}^{\lfloor \frac{h}{2^p} \rfloor \times \lfloor \frac{w}{2^p} \rfloor \times c}$, the K most recent feature maps are downsampled by a factor of 2×2 . Subsequently, the next group of K feature maps is downsampled by a 4×4 factor. This iterative procedure continues for subsequent groups, applying progressively larger downsampling factors, until the feature maps’ dimensions preclude further reduction. This approach is analogous to storing recent history at high resolution and distant history at increasingly lower resolutions. Assuming a single image comprises S tokens, the upper bound for the total token

count of memory features is derived as:

$$\frac{K}{4} \cdot S + \frac{K}{16} \cdot S + \frac{K}{64} \cdot S + \dots = \frac{K}{4} \left(\sum_{i=0}^{\infty} \frac{1}{4^i} \right) S = \frac{KS}{3}.$$

This approach facilitates a more effective token budget allocation. K is set 3, to ensure the total count for observation history does not exceed that of a single additional image.

Recursive Memory Representation A conventional strategy for mitigating token consumption is recursive memory, where a fixed-size state is iteratively updated. However, adapting this to MLLMs presents significant challenges. The primary difficulty stems from propagating gradients effectively through deep, multi-layer architectures across extended steps.

We introduce a novel approach that enables recursive memory modeling in MLLMs. Our intuition is to employ the KV cache of learnable tokens as the memory state. Specifically, the input prompt at time step t is structured as:

$$\{\mathbf{f}_t\}, \{\mathbf{m}_{pre}\}, \{\mathbf{w}\}, \{\mathbf{m}_{cur}\}$$

\mathbf{f}_t and \mathbf{w} denote the current visual representation and the instruction’s word embeddings, respectively. \mathbf{m}_{pre} serves as a placeholder for history memory, while \mathbf{m}_{cur} represents the learnable tokens used to compute the current memory state. As depicted in the Figure 2, within each transformer block of MLLM, the key-value (KV) states of the placeholder \mathbf{m}_{pre} are replaced by the KV states of $\{\mathbf{m}_{cur}\}$ computed at the previous step $t - \Delta$. During the forward pass at step t , the model processes this composite prompt. The learnable tokens $\{\mathbf{m}_{cur}\}$ attend to both the current inputs ($\{\mathbf{f}_t\}$, $\{\mathbf{w}\}$) and the past memory state (via $\{\mathbf{m}_{pre}\}$). This mechanism updates the internal states of $\{\mathbf{m}_{cur}\}$, integrating information from the current step and the historical context. The recursive process enables $\{\mathbf{m}_{cur}\}$ to function as an evolving memory state, propagating context forward across successive steps. Furthermore, utilizing the KV cache for learnable tokens, as opposed to output hidden states, mitigates the computational challenges associated with long-range gradient propagation during backpropagation.

In this paper, we adopt the progressive memory representation as the default configuration for our model. All main experiments, including comparisons with state-of-the-art methods, utilize this setup. We provide a detailed comparative analysis of the recursive memory representation in the experimental analysis section in Section 4.4.

3.4. Training Strategy

We follow StreamVLN [35] to employ a two-stage training strategy. The primary objective of the first stage is to equip the MLLM with fundamental navigation capabilities. Therefore, the model is trained on a mixed dataset of R2R-CE [19] and RxR-CE [21]. Different from StreamVLN, we

Algorithm 1 DAgger with Dynamic Mixed Policy

Require: Current policy π_θ , Oracle policy π^* , Dataset \mathcal{D}
Require: Set of environments \mathcal{E} , Decay rate α , Num trajectories N

```
1:  $\mathcal{D}_{\text{new}} \leftarrow \emptyset$ 
2: for  $i = 1 \rightarrow N$  do  $\triangleright$  Collect  $N$  new trajectories
3:   Sample env  $e \sim \mathcal{E}$  with state  $s_0$  and path length  $T$ 
4:    $t \leftarrow 0$ 
5:   while  $s_t$  is not terminal do
6:      $\beta_t \leftarrow 1 - \alpha^{t/T}$   $\triangleright$  Calculate dynamic oracle
       probability
7:      $a_t \sim \beta_t \pi^*(\cdot|s_t) + (1 - \beta_t) \pi_\theta(\cdot|s_t)$   $\triangleright$  Sample
       action to execute
8:      $a_t^* \leftarrow \pi^*(s_t)$   $\triangleright$  Get expert label for visited state
9:      $\mathcal{D}_{\text{new}} \leftarrow \mathcal{D}_{\text{new}} \cup \{(s_t, a_t^*)\}$ 
10:     $s_{t+1} \leftarrow \text{EnvironmentStep}(s_t, a_t)$ 
11:     $t \leftarrow t + 1$ 
12:   end while
13: end for
14:  $\mathcal{D}_{\text{agg}} \leftarrow \mathcal{D} \cup \mathcal{D}_{\text{new}}$   $\triangleright$  Aggregate datasets
15:  $\pi_{\theta_{\text{new}}} \leftarrow \text{Train}(\mathcal{D}_{\text{agg}})$   $\triangleright$  Train new policy
16: return  $\pi_{\theta_{\text{new}}}$ 
```

excluded the EnvDrop [28] dataset, as our preliminary studies indicate that extending the training steps on the mixed dataset yields greater performance benefits than incorporating the EnvDrop data.

In the second stage, we aim to enhance the model’s ability to correct errors, generalize to unseen environments, and follow instructions. This is achieved by augmenting the training corpus with additional data. First, we utilize ScaleVLN-150K [31] to improve generalization. Then, to enhance multimodal understanding, we incorporate multimodal question-answering datasets, including ScanQA [3], SQA3D [24], and a subset of LLaVA-Video-178K [45]. Finally, to specifically enhance error recovery, we introduce a dynamic mixed policy within the DAgger algorithm to collect valuable error-recovery data.

Improving DAgger with a Dynamic Mixed Policy. Previous work [19, 41, 43] employs the Dataset Aggregation (DAgger) [27] algorithm to enhance error recovery. DAgger collects off-policy trajectories by executing a mixed policy, which selects between the learned and oracle policy using a fixed probability β for the oracle policy. However, the choice of β introduces an exploration-efficiency trade-off. Specifically, a lower value of β drives a greater deviation from the correct path. This deviation is beneficial for learning to handle the test-time distribution shift and recovering from errors; however, it also results in substantially longer exploration trajectories, thereby increasing the training overhead. In contrast, a higher value of β tends to fol-

low the shortest path guided by the oracle policy, and is thus ineffective for enhancing error recovery.

To resolve this issue, we propose using a dynamic mixed policy to improve DAgger, as illustrated in Algorithm 1. To be specific, the probability β is dynamically adjusted as navigation progresses, determined by the following equation: $\beta = 1 - \alpha^{\frac{t}{T}}$, where α denotes a decay rate, t is the current time step, and T represents the total number of steps in the ground-truth path. β increases from 0 towards 1 as the navigation progresses, facilitating a gradual transition from the learned policy towards the oracle policy. Consequently, this design enables collecting exploratory trajectories without incurring excessive exploration lengths.

Training Acceleration via Sequence Packing. During training, a common step-by-step approach, which performs a separate forward pass per action step, leads to significant training overhead due to inefficient GPU utilization. To address this, we employ a sequence packing strategy that concatenates token sequences from multiple consecutive steps into a single flattened sequence. A block sparse attention mask¹ is then employed to confine attention computations to their respective steps. Furthermore, this concatenation strategy is crucial for our recursive memory representation, as it enables gradient backpropagation across steps. By adopting this method, we double the number of steps processed per backward pass (from 8 to 16), which reduces the total training overhead by 41.2%.

4. Experiments

4.1. Implementation and Training Details

Our model is built upon Qwen2.5-VL-3B [4] and utilizes StreamVGGT-1B [53] as the 3D geometry encoder. The progressive memory representation is used by default for training and evaluation unless specified otherwise. The temporal sampling stride Δ is set to 4, and the sliding window size N is set to 12. For both training stages, we employ the Adam optimizer with a batch size of 128 and a warmup ratio of 0.03. The learning rate is gradually increased to $1e-5$ during warmup before linearly decaying to 0. During training, we freeze the MLLM’s visual encoder, the 3D geometry encoder, and the multimodal connector, while leaving the MLLM backbone trainable. All experiments are conducted on 8 H800 80G GPUs.

Both the data collection and evaluation processes are conducted within the Habitat simulator. For the navigation task, we adopt the configuration from NaVILA [10], setting the visual observation resolution to 512×512 and the Horizontal Field of View (HFOV) to 90° . Each navigation episode terminates once the agent’s step count reaches the maximum of 500.

¹We adopt the Flex-FlashAttention implemented by [40].

Method	Observation Encoder				R2R-CE Val-Unseen				RxR-CE Val-Unseen			
	Pano.	Odo.	Depth	S.RGB	NE↓	OS↑	SR↑	SPL↑	NE↓	SR↑	SPL↑	nDTW↑
HPN+DN* [20]	✓	✓	✓		6.31	40.0	36.0	34.0	-	-	-	-
CMA* [13]	✓	✓	✓		6.20	52.0	41.0	36.0	8.76	26.5	22.1	47.0
VLN⊙BERT* [13]	✓	✓	✓		5.74	53.0	44.0	39.0	8.98	27.0	22.6	46.7
Sim2Sim* [18]	✓	✓	✓		6.07	52.0	43.0	36.0	-	-	-	-
GridMM* [32]	✓	✓	✓		5.11	61.0	49.0	41.0	-	-	-	-
ETPNav* [1]	✓	✓	✓		4.71	65.0	57.0	49.0	5.64	54.7	44.8	61.9
ScaleVLN* [31]	✓	✓	✓		4.80	-	55.0	51.0	-	-	-	-
InstructNav [23]	-	-	-	-	6.89	-	31.0	24.0	-	-	-	-
R2R-CMTP [5]	✓	✓	✓		7.90	38.0	26.4	22.7	-	-	-	-
LAW [26]		✓	✓	✓	6.83	44.0	35.0	31.0	10.90	8.0	8.0	38.0
CM2 [11]		✓	✓	✓	7.02	41.5	34.3	27.6	-	-	-	-
WS-MGMap [6]		✓	✓	✓	6.28	47.6	38.9	34.3	-	-	-	-
ETPNav + FF [33]		✓	✓	✓	5.95	55.8	44.9	30.4	8.79	25.5	18.1	-
Dynam3D [34]		✓	✓	✓	5.34	62.1	52.9	45.7	-	-	-	-
NaVid [41]				✓	5.47	49.1	37.4	35.9	-	-	-	-
NaVILA [10]				✓	5.37	57.6	49.7	45.5	-	-	-	-
StreamVLN [35]				✓	5.43	62.5	52.8	47.2	6.72	48.6	42.5	60.2
Efficient-VLN				✓	4.36	69.0	60.8	53.7	4.40	63.5	52.1	66.8
NaVILA† [10]				✓	5.22	62.5	54.0	49.0	6.77	49.3	44.0	58.8
UniNaVid† [43]				✓	5.58	53.3	47.0	42.7	6.24	48.7	40.9	-
StreamVLN† [35]				✓	4.98	64.2	56.9	51.9	6.22	52.9	46.0	61.9
NavFoM† [42]				✓	5.01	64.9	56.2	51.2	5.51	57.4	49.4	60.2
Efficient-VLN†				✓	4.18	73.7	64.2	55.9	3.88	67.0	54.3	68.4

Table 1. Comparison with state-of-the-art methods on R2R-CE and RxR-CE Val-Unseen split. The ‘‘Observation Encoder’’ inputs include panoramic (Pano.), odometry (Odo.), depth image (Depth), and single RGB image (S.RGB). * denotes methods utilizing the waypoint predictor from [13]. † denotes methods trained with additional data external to Matterport 3D.

	Training cost (hours)	# Samples	# Trajectories
UniNavid	1400 (H800)	3.6M	-
NaVILA	576 (A100)	1.5M	181K
StreamVLN	1500 (A100)	-	990K
NavFoM	4032 (H100)	12.7M	-
Efficient-VLN	282 (H800)	3.7M	196K

Table 2. Comparison of training costs and data volumes against other methods. #Samples denotes the count of (state, action) pairs, and #Trajectories is the number of navigation trajectories.

4.2. Evaluation Setup

Benchmarks. We evaluate our method on two widely used VLN benchmarks, *i.e.*, R2R-CE [19] and RxR-CE [21], both based on the Habitat simulator. R2R-CE comprises 4,475 trajectories, split into 3,862 for training and 613 for the val-unseen split, with each trajectory accompanied by three natural language instructions. RxR-CE includes 14,005 trajectories, consisting of 10,336 for training and 3,669 for the val-unseen split.

Metrics. We employ the following metrics: 1) Navigation Error (NE), which measures the average distance between the agent’s final location and the destination; 2) Success

Rate (SR), the percentage of the episodes where the agent stops within a predefined distance threshold of the target; 3) Oracle Success Rate (OSR), the SR given an oracle stopping policy; 4) Success rate weighted by the Path Length (SPL), the SR weighted by the ratio of the ground truth length to the agent’s path length; 5) normalized Dynamic Time Warping (nDTW) [17], which applies time warping to measure the alignment between the agent’s trajectory and ground truth path.

4.3. Quantitative Results

Table 1 compares our model with state-of-the-art methods on R2R-CE and RxR-CE Val-Unseen benchmarks. We first evaluate our method trained without external navigation data. Efficient-VLN achieves an SR of 60.8% on R2R-CE and 63.5% on RxR-CE, outperforming the previous state-of-the-art StreamVLN by 8.0% and 14.9%, respectively. When further incorporating the ScaleVLN-150K dataset, our model sets a new state-of-the-art, achieving an SR of 64.2 on R2R-CE and an SR of 67.0 on RxR-CE.

Table 2 compares the training costs and data volumes with those of competing methods. Notably, our method requires only 282 H800 GPU hours, a significantly lower training cost than prior state-of-the-art models, highlighting the training efficiency of our proposed approach.

#		R2R-CE Val-Unseen					RxR-CE Val-Unseen				
		NE↓	OS↑	SR↑	SPL↑	#Token	NE↓	SR↑	SPL↑	nTDW↑	#Token
1	Spatial Compression (all frames)	4.79	66.9	55.9	48.8	499	5.13	58.6	47.6	64.1	606
2	Recursive Memory (64 tokens)	4.65	66.6	56.1	49.4	586	5.46	54.7	45.3	63.8	677
3	Prog. Spatial Compression (3 frames)	4.47	67.5	58.5	52.3	661	4.71	61.9	50.6	65.1	745
4	Prog. Spatial Compression (6 frames)	4.23	69.4	61.3	55.1	692	4.44	62.4	51.3	66.5	780
5	Prog. Spatial Compression (12 frames)	4.36	69.0	60.8	53.7	701	4.40	63.5	52.1	66.8	785

Table 3. Comparison of different memory modeling strategies. “#Token” denotes the average token count per forward pass during navigation. The ScaleVLN dataset is excluded from these experiments.

#		R2R-CE Val-Unseen						RxR-CE Val-Unseen					
		NE↓	OS↑	SR↑	SPL↑	#Train Step	#Infer Step	NE↓	SR↑	SPL↑	nDTW↑	#Train Step	#Infer Step
1	Baseline (w/o DAgger)	6.41	54.5	45.9	41.9	–	83	6.51	49.8	41.5	59.4	–	137
2	Constant Ratio ($\beta = 0.75$)	5.77	57.1	50.7	46.7	66	84	5.71	54.1	46.4	64.2	98	126
3	Constant Ratio ($\beta = 0.5$)	4.95	61.5	54.8	49.5	78	94	4.79	60.7	50.7	69.0	112	142
4	Constant Ratio ($\beta = 0.25$)	3.97	69.6	59.5	52.1	128	146	4.01	62.6	51.6	67.7	160	186
5	Dynamic Ratio ($\alpha = 0.5$)	4.36	69.0	60.8	53.7	82	100	4.40	63.5	52.1	66.8	121	154

Table 4. Effect of DAgger algorithm. #Train Step represents the average length of collected trajectories. #Infer Step is the average length of predicted trajectories during inference. The ScaleVLN dataset is excluded from the experiments.

4.4. Analysis

Effect of Memory Representation. We present the comparison of different memory representations in Table 3. Specifically, we investigate the following variants. 1) “Recursive Memory”: We use the KV cache of 64 learnable tokens as the recursive memory representation. 2) “Spatial Compression”: Following the prior work [41], we compress each image into four tokens. 3) “Prog. Spatial Compression”: we retain the n most recent images ($n \in \{3, 6, 12\}$) and employ the progressive spatial compression to encode them into the memory. For all variants, video frames are sampled with a stride of four. In addition to standard navigation metrics, we also report the average token count per forward pass (#Token) during navigation.

“Recursive Memory” (row 2) obtains 56.1 SR on R2R-CE and 54.7 SR on RxR-CE, which is highly competitive with the previous state-of-the-art, StreamVLN (52.8 SR on R2R-CE, 48.6 on RxR-CE). Comparing rows 1 and 2, we observe that while “Recursive Memory” outperforms on R2R-CE, it underperforms in RxR-CE. Given that RxR-CE features longer trajectories, this indicates that the “Recursive Memory” struggles to retain essential information over long sequences. Comparing rows 1 and 3, “Prog. Spatial Compression (3 frames)” significantly surpasses “Spatial Compression” by 2.6 SR on R2R-CE and 3.0 SR on RxR-CE. This highlights the importance of recent visual history, suggesting that aggressively compressing this memory (as in row 1) hinders performance. Increasing frames from 3 to 6 (rows 3 vs. 4) yields significant improvements across all

metrics, while only increasing the average token count by ~ 30 . Further increasing frames to 12 (row 5) continues to improve performance on RxR-CE, though it incurs a minor performance drop on R2R-CE. These findings suggest that the progressive memory is particularly effective for long-horizon navigation, as evidenced by the consistent gains on the longer-trajectory RxR-CE dataset.

Effect of DAgger Algorithm We further investigate the effect of the DAgger algorithm in Table 4. “Baseline” denotes the model trained without DAgger data. “Constant ratio” applies a fixed mixing ratio β for selecting the oracle policy, while “Dynamic ratio” employs a dynamic mixing ratio. Comparing rows 1 and 2, incorporating the DAgger data yields a significant improvement, boosting SR from 45.9 to 50.7 on R2R-CE, and from 49.8 to 54.1 on RxR-CE. Further reducing the mixing ratio β (rows 2-4) yields continued performance improvements. Specifically, decreasing β from 0.75 to 0.25 improves SR by 8.8 points (50.7 to 59.5) on R2R-CE and 8.5 points (54.1 to 62.6) on RxR-CE. This is because a lower β encourages the agent to explore more diverse, error-prone trajectories. However, this improvement comes at a cost. The average length of collected trajectories (#Train Step) also increases significantly, from 66 (row 2) to 128 (row 4) on R2R-CE. Not only does the training overhead increase due to the excessively long training trajectories, but so does the length of the inferred paths (#Infer Step). These results demonstrate a clear trade-off between success rate and trajectory length.

The “Dynamic ratio” (row 5) achieves the highest SR

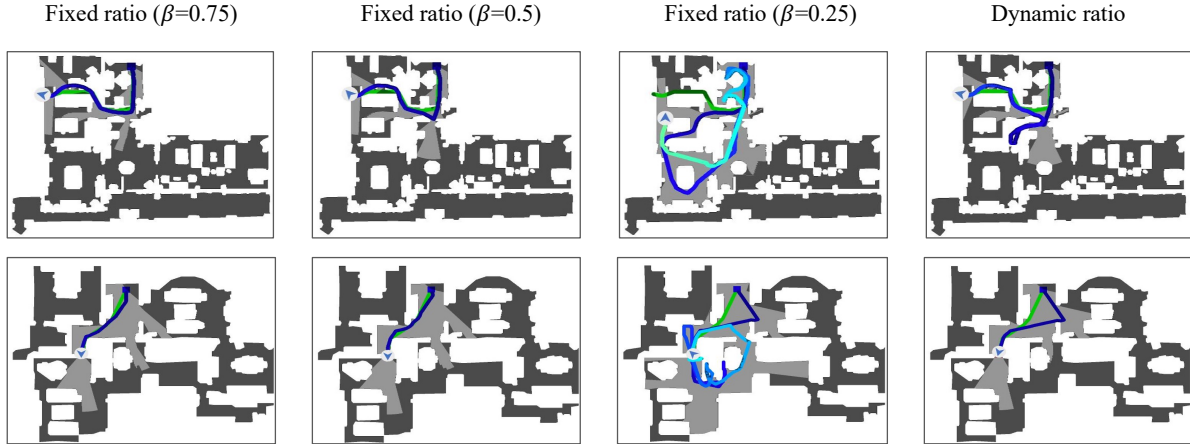


Figure 3. Visualization of the DAGger-generated trajectories. The green lines denote ground truth trajectories, and the blue lines denote predicted trajectories.

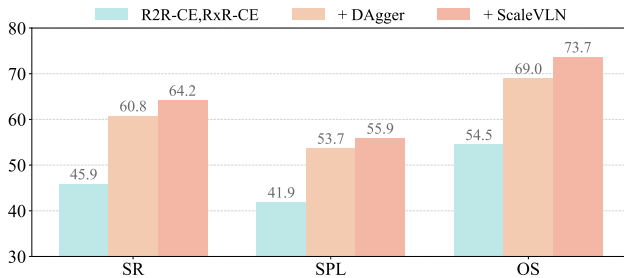


Figure 4. Ablation study of data composition on R2R-CE. The baseline (R2R, RxR) is progressively augmented with DAGger data (+ DAGger) and the ScaleVLN dataset (+ ScaleVLN).

and SPL on both R2R-CE and RxR-CE, surpassing even the best-performing constant ratio (row 4). Crucially, it achieves this with a much lower exploration length, reducing the #Train Step from 128 to 82 on R2R-CE, and from 160 to 121 on RxR-CE.

Visualization for DAGger-generated trajectories. Figure 3 visualizes the BEV map of trajectories generated by DAGger. A high fixed ratio (*e.g.*, $\beta = 0.75$) leads to trajectories composed predominantly of oracle actions, yielding ineffective error-recovery data. Conversely, a low fixed ratio (*e.g.*, $\beta = 0.25$) allows the agent to deviate from the expert path frequently, but leads to long exploration paths. Our dynamic ratio resolves this trade-off, thus collecting valuable error-recovery data while avoiding excessive exploration.

Ablation Study of Data Composition. We then investigate the impact of data composition. Specifically, we compare the model after stage 1 (trained on R2R-CE, RxR-CE) with models fine-tuned in stage 2 by gradually incorporating the DAGger and ScaleVLN data into the training data. As shown in Figure 4, the baseline (“R2R-CE, RxR-CE”)

	NE↓	OS↑	SR↑	SPL↑
2D tokens only	6.80	50.7	42.3	38.4
+ StreamVGGT [53]	6.41	54.5	45.9	41.9
+ Stream3R [22]	6.39	55.5	47.1	42.6

Table 5. Effect of the 3D geometry encoder on R2R-CE. All models are trained with first stage only.

achieves an SR of 45.9 and an SPL of 41.9. Incorporating the DAGger data brings the most significant improvement, boosting SR to 60.8 and SPL to 53.7. Finally, including the ScaleVLN data further enhances performance to 64.2 SR and 55.9 SPL.

Effect of 3D Geometry. To evaluate the impact of 3D geometry, we compare StreamVGGT [53] and Stream3R [22]. As shown in Table 5, StreamVGGT and Stream3R yield improvements of 3.9% and 4.8% in SR, respectively. Although Stream3R performs slightly better, we adopt StreamVGGT for its lower memory cost during training.

5. Conclusion

In this paper, we address the substantial training cost of MLLM-based Vision-Language Navigation (VLN) by proposing **Efficient-VLN**, a training-efficient VLN model. Efficient-VLN introduces two key innovations: (1) efficient memory representations (progressive and recursive) to mitigate the quadratic computational burden of extensive observations, and (2) a dynamic mixed policy to balance the exploration-efficiency trade-off. Experiments demonstrate that Efficient-VLN achieves new state-of-the-art performance on both R2R-CE (62.3% SR) and RxR-CE (64.5% SR), using merely 282 H800 GPU hours, providing a strong and efficient baseline for this area.

References

- [1] Dong An, Hanqing Wang, Wenguan Wang, Zun Wang, Yan Huang, Keji He, and Liang Wang. Etpnav: Evolving topological planning for vision-language navigation in continuous environments. *TPAMI*, 2023. 6
- [2] Peter Anderson, Qi Wu, Damien Teney, Jake Bruce, Mark Johnson, Niko Sünderhauf, Ian Reid, Stephen Gould, and Anton Van Den Hengel. Vision-and-language navigation: Interpreting visually-grounded navigation instructions in real environments. In *CVPR*, 2018. 1, 2, 11
- [3] Daichi Azuma, Taiki Miyayoshi, Shuhei Kurita, and Motoaki Kawanabe. Scanqa: 3d question answering for spatial scene understanding. In *CVPR*, 2022. 5, 11, 12
- [4] Shuai Bai, Keqin Chen, Xuejing Liu, Jialin Wang, Wenbin Ge, Sibao Song, Kai Dang, Peng Wang, Shijie Wang, Jun Tang, et al. Qwen2. 5-vl technical report. *arXiv preprint arXiv:2502.13923*, 2025. 3, 5, 11
- [5] Kevin Chen, Junshen K Chen, Jo Chuang, Marynel Vázquez, and Silvio Savarese. Topological planning with transformers for vision-and-language navigation. In *CVPR*, 2021. 1, 2, 6
- [6] Peihao Chen, Dongyu Ji, Kunyang Lin, Runhao Zeng, Thomas H Li, Mingkui Tan, and Chuang Gan. Weakly-supervised multi-granularity map learning for vision-and-language navigation. *arXiv preprint arXiv:2210.07506*, 2022. 6
- [7] Shizhe Chen, Pierre-Louis Guhur, Makarand Tapaswi, Cordelia Schmid, and Ivan Laptev. Think global, act local: Dual-scale graph transformer for vision-and-language navigation. In *CVPR*, 2022. 1, 2
- [8] Sijin Chen, Xin Chen, Chi Zhang, Mingsheng Li, Gang Yu, Hao Fei, Hongyuan Zhu, Jiayuan Fan, and Tao Chen. Ll3da: Visual interactive instruction tuning for omni-3d understanding reasoning and planning. In *CVPR*, 2024. 12
- [9] An-Chieh Cheng, Yang Fu, Yukang Chen, Zhijian Liu, Xiaolong Li, Subhashree Radhakrishnan, Song Han, Yao Lu, Jan Kautz, Pavlo Molchanov, et al. 3d aware region prompted vision language model. *arXiv preprint arXiv:2509.13317*, 2025. 2
- [10] An-Chieh Cheng, Yandong Ji, Zhaojing Yang, Zaitian Gongye, Xueyan Zou, Jan Kautz, Erdem Bıyık, Hongxu Yin, Sifei Liu, and Xiaolong Wang. Navila: Legged robot vision-language-action model for navigation. *Robotics: Science and Systems*, 2025. 1, 2, 3, 4, 5, 6, 12
- [11] Georgios Georgakis, Karl Schmeckpeper, Karan Wanchoo, Soham Dan, Eleni Miltsakaki, Dan Roth, and Kostas Daniilidis. Cross-modal map learning for vision and language navigation. In *CVPR*, 2022. 6
- [12] Yicong Hong, Qi Wu, Yuankai Qi, Cristian Rodriguez-Opazo, and Stephen Gould. Vln bert: A recurrent vision-and-language bert for navigation. In *CVPR*, 2021. 2
- [13] Yicong Hong, Zun Wang, Qi Wu, and Stephen Gould. Bridging the gap between learning in discrete and continuous environments for vision-and-language navigation. In *CVPR*, 2022. 2, 6
- [14] Yining Hong, Haoyu Zhen, Peihao Chen, Shuhong Zheng, Yilun Du, Zhenfang Chen, and Chuang Gan. 3d-llm: Injecting the 3d world into large language models. In *NeurIPS*, 2023. 12
- [15] Haifeng Huang, Yilun Chen, Zehan Wang, Rongjie Huang, Runsen Xu, Tai Wang, Luping Liu, Xize Cheng, Yang Zhao, Jiangmiao Pang, et al. Chat-scene: Bridging 3d scene and large language models with object identifiers. In *NeurIPS*, 2024. 12
- [16] Jianguo Huang, Silong Yong, Xiaojian Ma, Xiongkun Linghu, Puhao Li, Yan Wang, Qing Li, Song-Chun Zhu, Baoxiong Jia, and Siyuan Huang. An embodied generalist agent in 3d world. In *ICML*, 2024. 12
- [17] Gabriel Ilharco, Vihan Jain, Alexander Ku, Eugene Ie, and Jason Baldridge. General evaluation for instruction conditioned navigation using dynamic time warping. 2019. 6
- [18] Jacob Krantz and Stefan Lee. Sim-2-sim transfer for vision-and-language navigation in continuous environments. In *ECCV*, 2022. 6
- [19] Jacob Krantz, Erik Wijmans, Arjun Majumdar, Dhruv Batra, and Stefan Lee. Beyond the nav-graph: Vision and language navigation in continuous environments. In *ECCV*, 2020. 1, 2, 4, 5, 6
- [20] Jacob Krantz, Aaron Gokaslan, Dhruv Batra, Stefan Lee, and Oleksandr Maksymets. Waypoint models for instruction-guided navigation in continuous environments. In *ICCV*, 2021. 1, 2, 6
- [21] Alexander Ku, Peter Anderson, Roma Patel, Eugene Ie, and Jason Baldridge. Room-across-room: Multilingual vision-and-language navigation with dense spatiotemporal grounding. In *EMNLP*, 2020. 1, 2, 4, 6, 11
- [22] Yushi Lan, Yihang Luo, Fangzhou Hong, Shangchen Zhou, Honghua Chen, Zhaoyang Lyu, Shuai Yang, Bo Dai, Chen Change Loy, and Xingang Pan. Stream3r: Scalable sequential 3d reconstruction with causal transformer, 2025. 3, 8
- [23] Yuxing Long, Wenzhe Cai, Hongcheng Wang, Guanqi Zhan, and Hao Dong. Instructnav: Zero-shot system for generic instruction navigation in unexplored environment. *arXiv preprint arXiv:2406.04882*, 2024. 1, 2, 6
- [24] Xiaojian Ma, Silong Yong, Zilong Zheng, Qing Li, Yitao Liang, Song-Chun Zhu, and Siyuan Huang. Sqa3d: Situated question answering in 3d scenes. In *ICLR*, 2023. 5, 11, 12
- [25] Yuankai Qi, Qi Wu, Peter Anderson, Xin Wang, William Yang Wang, Chunhua Shen, and Anton van den Hengel. Reverie: Remote embodied visual referring expression in real indoor environments. In *CVPR*, 2020. 1, 2
- [26] Sonia Raychaudhuri, Saim Wani, Shivansh Patel, Unnat Jain, and Angel X Chang. Language-aligned waypoint (law) supervision for vision-and-language navigation in continuous environments. *arXiv preprint arXiv:2109.15207*, 2021. 6
- [27] Stéphane Ross, Geoffrey Gordon, and Drew Bagnell. A reduction of imitation learning and structured prediction to no-regret online learning. In *AISTATS*, 2011. 5, 11
- [28] Hao Tan, Licheng Yu, and Mohit Bansal. Learning to navigate unseen environments: Back translation with environmental dropout. In *NAACL*, 2019. 2, 5
- [29] Jesse Thomason, Michael Murray, Maya Cakmak, and Luke Zettlemoyer. Vision-and-dialog navigation. In *CoRL*. PMLR, 2020. 1, 2

- [30] Jianyuan Wang, Minghao Chen, Nikita Karaev, Andrea Vedaldi, Christian Rupprecht, and David Novotny. Vggt: Visual geometry grounded transformer. In *CVPR*, 2025. 3
- [31] Zun Wang, Jialu Li, Yicong Hong, Yi Wang, Qi Wu, Mohit Bansal, Stephen Gould, Hao Tan, and Yu Qiao. Scaling data generation in vision-and-language navigation. In *ICCV*, 2023. 2, 5, 6, 11
- [32] Zihan Wang, Xiangyang Li, Jiahao Yang, Yeqi Liu, and Shuqiang Jiang. Gridmm: Grid memory map for vision-and-language navigation. In *ICCV*, 2023. 2, 6
- [33] Zihan Wang, Xiangyang Li, Jiahao Yang, Yeqi Liu, and Shuqiang Jiang. Sim-to-real transfer via 3d feature fields for vision-and-language navigation. *arXiv preprint arXiv:2406.09798*, 2024. 6
- [34] Zihan Wang, Seungjun Lee, and Gim Hee Lee. Dynam3d: Dynamic layered 3d tokens empower vlm for vision-and-language navigation. In *NeurIPS*, 2025. 2, 6
- [35] Meng Wei, Chenyang Wan, Xiqian Yu, Tai Wang, Yuqiang Yang, Xiaohan Mao, Chenming Zhu, Wenzhe Cai, Hanqing Wang, Yilun Chen, et al. Streamvln: Streaming vision-and-language navigation via slowfast context modeling. *arXiv preprint arXiv:2507.05240*, 2025. 1, 2, 3, 4, 6, 11, 12
- [36] Diankun Wu, Fangfu Liu, Yi-Hsin Hung, and Yueqi Duan. Spatial-mllm: Boosting mllm capabilities in visual-based spatial intelligence. In *NeurIPS*, 2025. 3
- [37] Jihan Yang, Shusheng Yang, Anjali W Gupta, Rilyn Han, Li Fei-Fei, and Saining Xie. Thinking in space: How multimodal large language models see, remember, and recall spaces. In *CVPR*, 2025. 2
- [38] Zhuoyuan Yu, Yuxing Long, Zihan Yang, Chengyan Zeng, Hongwei Fan, Jiyao Zhang, and Hao Dong. Correctnav: Self-correction flywheel empowers vision-language-action navigation model. *arXiv preprint arXiv:2508.10416*, 2025. 2
- [39] Shuang Zeng, Dekang Qi, Xinyuan Chang, Feng Xiong, Shichao Xie, Xiaolong Wu, Shiyi Liang, Mu Xu, and Xing Wei. Janusvln: Decoupling semantics and spatiality with dual implicit memory for vision-language navigation, 2025. 3
- [40] Tao Zewei and Huang Yunpeng. Magiattention: A distributed attention towards linear scalability for ultra-long context, heterogeneous mask training. <https://github.com/SandAI-org/MagiAttention/>, 2025. 5, 11
- [41] Jiazhao Zhang, Kunyu Wang, Rongtao Xu, Gengze Zhou, Yicong Hong, Xiaomeng Fang, Qi Wu, Zhizheng Zhang, and He Wang. Navid: Video-based vlm plans the next step for vision-and-language navigation. *Robotics: Science and Systems*, 2024. 1, 2, 3, 4, 5, 6, 7, 11
- [42] Jiazhao Zhang, Anqi Li, Yunpeng Qi, Minghan Li, Jiahang Liu, Shaoan Wang, Haoran Liu, Gengze Zhou, Yuze Wu, Xingxing Li, et al. Embodied navigation foundation model. *arXiv preprint arXiv:2509.12129*, 2025. 1, 6
- [43] Jiazhao Zhang, Kunyu Wang, Shaoan Wang, Minghan Li, Haoran Liu, Songlin Wei, Zhongyuan Wang, Zhizheng Zhang, and He Wang. Uni-navid: A video-based vision-language-action model for unifying embodied navigation tasks. *Robotics: Science and Systems*, 2025. 1, 2, 3, 4, 5, 6, 11
- [44] Kaichen Zhang, Bo Li, Peiyuan Zhang, Fanyi Pu, Joshua Adrian Cahyono, Kairui Hu, Shuai Liu, Yuanhan Zhang, Jingkang Yang, Chunyuan Li, et al. Lmms-eval: Reality check on the evaluation of large multimodal models. In *Findings of the Association for Computational Linguistics: NAACL 2025*, 2025. 11
- [45] Yuanhan Zhang, Jinming Wu, Wei Li, Bo Li, Zejun Ma, Ziwei Liu, and Chunyuan Li. Video instruction tuning with synthetic data. *arXiv preprint arXiv:2410.02713*, 2024. 5, 11
- [46] Duo Zheng, Shijia Huang, Lin Zhao, Yiwu Zhong, and Liwei Wang. Towards learning a generalist model for embodied navigation. In *CVPR*, 2024. 1, 2, 12
- [47] Duo Zheng, Shijia Huang, Yanyang Li, and Liwei Wang. Learning from videos for 3d world: Enhancing mllms with 3d vision geometry priors. In *NeurIPS*, 2025. 2, 3
- [48] Duo Zheng, Shijia Huang, and Liwei Wang. Video-3d llm: Learning position-aware video representation for 3d scene understanding. In *CVPR*, 2025. 2, 12
- [49] Gengze Zhou, Yicong Hong, and Qi Wu. Navgpt: Explicit reasoning in vision-and-language navigation with large language models. In *AAAI*, 2024. 1, 2
- [50] Chenming Zhu, Tai Wang, Wenwei Zhang, Jiangmiao Pang, and Xihui Liu. Llava-3d: A simple yet effective pathway to empowering llms with 3d-awareness. In *ICCV*, 2025. 12
- [51] Ziyu Zhu, Xiaojian Ma, Yixin Chen, Zhidong Deng, Siyuan Huang, and Qing Li. 3d-vista: Pre-trained transformer for 3d vision and text alignment. In *CVPR*, 2023. 12
- [52] Ziyu Zhu, Xilin Wang, Yixuan Li, Zhuofan Zhang, Xiaojian Ma, Yixin Chen, Baoxiong Jia, Wei Liang, Qian Yu, Zhidong Deng, et al. Move to understand a 3d scene: Bridging visual grounding and exploration for efficient and versatile embodied navigation. In *ICCV*, 2025. 2
- [53] Dong Zhuo, Wenzhao Zheng, Jiahe Guo, Yuqi Wu, Jie Zhou, and Jiwen Lu. Streaming 4d visual geometry transformer. *arXiv preprint arXiv:2507.11539*, 2025. 2, 3, 5, 8

Efficient-VLN: A Training-Efficient Vision-Language Navigation Model

Supplementary Material

1. Additional Implementation Details

Training Details. Our implementation is built upon the official Qwen2.5-VL [4] codebase. To adapt this framework for the VLN task, we implement a custom dataset module that processes navigation steps sequentially, rather than treating them as independent instances. For training efficiency, we group navigation trajectories by length, with trajectories in each group padded to the group’s maximum length. Each group is then distributed across different processes to enable multi-GPU acceleration. To enhance GPU parallelism, we split each trajectory’s state-action pairs into consecutive chunks, each containing 16 steps. Within each segment, textual prompts are concatenated into a single, flattened prompt, while block-sparse attention [40] is employed to restrict computations to their corresponding steps.

For video question-answering and video instruction tuning data, we uniformly sample 16 frames from each video.

Dagger Process. The Dataset Aggregation (Dagger) [27] algorithm iteratively collects new trajectories and aggregates them into the existing dataset to bootstrap the model. Specifically, this process involves utilizing a mixed policy of the learned policy and oracle policy to generate the trajectories, which are then relabeled with expert actions. This approach has been widely adopted by recent MLLM-based methods [35, 41, 43] to enhance error recovery capabilities, typically employing only a single iteration of data collection. Following this convention, we also adopt a single-iteration setting.

To accommodate our model’s prediction horizon of four actions, we adapted the standard Dagger implementation. Specifically, at a given state, we first advance the oracle policy by four steps to obtain the corresponding sequence of expert actions. We subsequently revert the environment to the original state and proceed with trajectory generation under the mixed policy.

Evaluation Details For VLN, our code is built upon the evaluation code of StreamVLN [35]. Specifically, during the RxR evaluation, since certain samples yield “N/A” values for SPL, we follow StreamVLN [35] to set those invalid metrics to 0 for metric computation. For 3D question-answering benchmarks such as ScanQA [3] and SQA3D [24], our evaluation code is built upon the LMMs-Eval [44] framework. During inference, we uniformly sample 16 frames from each scene as input.

	#Count	#State-Action Pairs
R2R	10,819	153,693
RxR	19,894	467,807
Dagger (R2R)	10,819	218,129
Dagger (RxR)	19,672	588,589
ScaleVLN-150K	155,098	1,821,560
SQA3D	26,623	–
ScanQA	26,515	–
LLaVA-Video-178K (subset)	48,468	–

Table 6. Statistics of the combined dataset. #Count denotes the number of samples for VLN, Video QA, and multimodal instruction tuning tasks. #State-Action Pairs refers to the number of state-action pairs in VLN samples, where trajectories are sampled with a stride of 4.

2. Data Statistics

Our training data statistics are presented in Table 6. The dataset spans three categories: Vision-Language Navigation (VLN), 3D question-answering, and video instruction tuning. For VLN datasets (e.g., R2R [2], RxR [21], ScaleVLN [31]), we convert trajectories into state-action pairs with a stride of 4. Non-navigation tasks, including SQA3D [24], ScanQA [3], and a subset of LLaVA-Video-178K [45], are included to improve the model’s generalizability.

3. Results on 3D Question Answering

To investigate the spatial understanding capabilities of our model, we conduct experiments on two widely used 3D question-answering benchmarks: SQA3D [24] and ScanQA [3]. The comparison results for SQA3D and ScanQA are presented in Table 7 and Table 8, respectively. These results demonstrate that our method achieves performance highly competitive with leading methods.

Method	Venue	Test set						Avg.
		What	Is	How	Can	Which	Others	
Expert Models								
SQA3D [24]	ICLR 2023	31.6	63.8	46.0	69.5	43.9	45.3	46.6
3D-VisTA [51]	ICCV 2023	34.8	63.3	45.4	69.8	47.2	48.1	48.5
3D Large Language Models								
LEO [16]	ICML 2024	–	–	–	–	–	–	50.0
ChatScene [15]	NeurIPS 2024	45.4	67.0	52.0	69.5	49.9	55.0	54.6
LLaVA-3D [50]	ICCV 2025	–	–	–	–	–	–	55.6
Video-3D LLM [48]	CVPR 2025	51.1	72.4	55.5	69.8	51.3	56.0	58.6
2D Vision-Language-Action Models								
Efficient-VLN	–	46.9	71.8	54.4	72.5	45.6	55.1	56.2

Table 7. Performance comparison on the test set of SQA3D [24].

Method	Venue	EM	B-1	B-2	B-3	B-4	ROUGE-L	METEOR	CIDEr
Expert Models									
ScanQA [3]	CVPR22	21.05	30.24	20.40	15.11	10.08	33.33	13.14	64.86
3D-VisTA [51]	ICCV23	22.4	–	–	–	10.4	35.7	13.9	69.6
3D large Language Models									
3D-LLM (Flamingo) [14]	NeurIPS23	20.4	30.3	17.8	12.0	7.2	32.3	12.2	59.2
3D-LLM (BLIP2-flant5) [14]	NeurIPS23	20.5	39.3	25.2	18.4	12.0	35.7	14.5	69.4
LL3DA [8]	CVPR24	–	–	–	–	13.53	37.31	15.88	76.79
LEO [16]	ICML24	–	–	–	–	11.5	39.3	16.2	80.0
ChatScene [15]	NeurIPS24	21.62	43.20	29.06	20.57	14.31	41.56	18.00	87.70
LLaVA-3D [50]	ICCV25	27.0	–	–	–	14.5	50.1	20.7	91.7
Video-3D LLM [48]	–	30.10	47.05	31.70	22.83	16.17	49.02	19.84	102.06
2D Vision-Language-Action Models									
NaviLLM [46]	CVPR24	23.0	–	–	–	12.5	38.4	15.4	75.9
NaVILA (16 frames) [10]	RSS25	27.4	–	–	–	15.2	48.3	19.6	99.8
StreamVLN (16 frames) [35]	–	28.8	–	–	–	15.7	48.3	19.8	100.2
Efficient-VLN	–	28.3	45.1	30.6	22.5	16.2	46.2	18.7	95.6

Table 8. Performance comparison on the validation set of ScanQA [3]. EM indicates exact match accuracy, and B-1, B-2, B-3, B-4 denote BLEU-1, -2, -3, -4, respectively.